EurJOC European Journal of Organic Chemistry

FULL PAPER

DOI: 10.1002/ejoc.201500602

Fluoren-9-ylidene-Based Dyes for Dye-Sensitized Solar Cells

Alexis Tigreros,[a] Danisha M. Rivera-Nazario,[b] Alejandro Ortiz,[a] Nazario Martin,[c] Braulio Insuasty,*[a] and Luis A. Echegoyen*[b]

Keywords: Dye-sensitized solar cells / Fused-ring systems / Electrochemistry / Impedance spectroscopy / Density functional calculations

Three new dyes (**1**–**3**) with a triarylamine electron donor, a cyanoacrylic acid moiety as both electron acceptor and anchoring group, and a fluorene-9-ylidene moiety as an antenna were synthesized, and their electrochemical, photophysical, and photovoltaic properties were evaluated. Despite minor differences in absorption properties, as the starburst shape of the dyes increases and highly hindered hydrophobic groups are introduced, the measured open-cell voltage (V_{oc}) increased noticeably from 0.79 to 0.83 V, and the power-conversion efficiency (PCE) value increased from 3.98 to 4.73 %.

Introduction

The generation of clean and renewable energy is one of the most important scientific and technological challenges of the 21st century. As sunlight is the most abundant source of readily available energy,[1] organic solar cells, particularly dye-sensitized solar cells (DSSCs), appear to be a highly promising and cost-effective alternative for photovoltaic technologies.[2]

DSSCs are electrochemical devices that use light-absorbing dye molecules attached to semiconductor nanoparticles that convert sunlight into electrical energy.[3] In this type of photovoltaic device, the sensitizer absorbs the light and injects electrons into the conduction band of the semiconductor.[4] Presently, the most efficient photosensitizers are ruthenium-[5] and porphyrin-based dyes.[6] However, these chromophores are expensive and difficult to prepare in high yields. Thus, the design of metal-free compounds for DSSCs is an active field in materials science,[7] and numerous reports concerning the photophysical, photochemical, and electrochemical properties of the dyes have appeared. The donor–π-bridge–acceptor (D–π-B–A) model is the most common strategy utilized.[8] Much progress has been made in recent years by using different chromophores with D–π-B–A architectures containing coumarin,[9] indoline,[10] rhodanine,[11] and triarylamine groups.[12]

To achieve high conversion efficiencies, one of the most important requirements is that the sensitizer absorbs as much incoming sunlight as possible. One strategy towards this end is the introduction of more π-conjugated segments between the donor and the acceptor. However, the elongation with rod- or disk-shaped molecules can lead to the recombination of the photoinduced electrons with the triiodide electrolyte and to the formation of aggregates between dye molecules.[13]

The effective suppression of recombination processes [between the injected electrons and triiodide (I_3^-) ions in the electrolyte], dark current, and the aggregation processes of dye molecules leads to increased open-circuit voltage (V_{oc}) values and consequently to better overall solar-cell performances. To achieve these goals, coadsorbents such as *tert*-butylpyridine (TBP)[14] and deoxycholic acid (DCA)[15] have been used. However, the use of additives decreases the amount of adsorbed dye on the TiO_2 surface and, thus, lowers the photoconversion.[16] Other strategies to inhibit these processes and to improve the V_{oc} values involve the incorporation of starburst molecules,[16] long alkyl chains,[17] fluorinated alkyl chains,[18] and dendritic molecules.[19] Fluoren-9-ylidene-based compounds have been used in high-efficiency polymer solar cells[20] and, more recently, in DSSCs.[16,21]

On the basis of these considerations, we designed and synthesized three new dyes, **1**–**3**, by extending the starburst shape of triarylamine–cyanoacrylic chromophores with fluorene-9-ylidene moieties as antennas (Figure 1). We anticipated that the introduction of a highly hindered alkyl group such as (triisopropylsilyl)acetylene would improve the overall DSSC device performance. Furthermore, as the conjugation with a fluorene moiety would increase electron delocalization and the electron-donating ability of the triarylamine group, we decided to increase the distance between the

[a] Departamento de Química, Universidad del Valle, Cali, AA 25360, Colombia
http://gich.correounivalle.edu.co
[b] Department of Chemistry, University of Texas at El Paso, 500 W University Ave, El Paso, TX 79968, USA
E-mail: echegoyen@utep.edu
http://science.utep.edu/echegoyen/
[c] Departamento de Química Orgánica, Universidad Complutense, 28040 Madrid, Spain

Supporting information for this article is available on the WWW under http://dx.doi.org/10.1002/ejoc.201500602.

fluorene moiety and the triarylamine group by introducing an additional vinyl group to avoid steric repulsion.

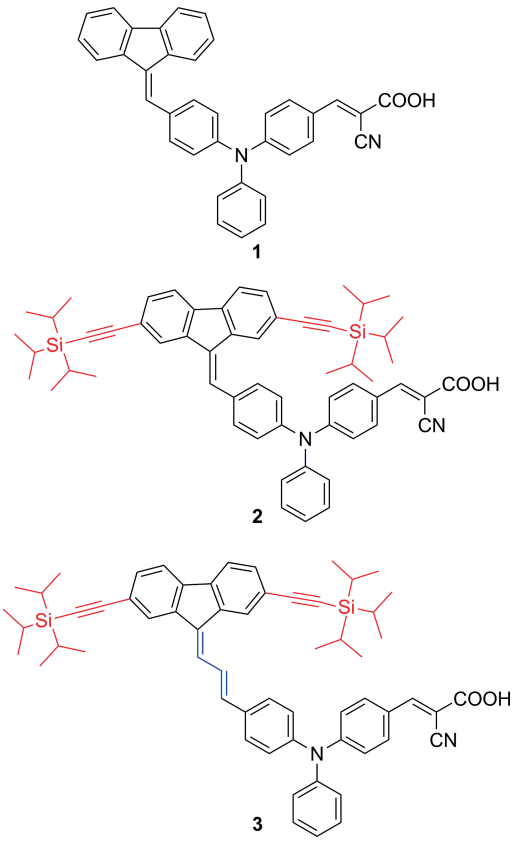

Figure 1. Structure of dyes **1**–**3**.

Results and Discussion

Synthetic Procedures

The syntheses of the sensitizers **1**–**3** were achieved in two (**1**), three (**2**), and four (**3**) steps by the synthetic pathways described in Scheme 1. The starting compounds **4** and **10** were prepared according to reported procedures, and the analytical data are presented in the Supporting Information. Aldehydes **6** and **8** were prepared by the condensation of **4** with fluorene (**5**) and 2,7-dibromofluorene (**7**), respectively, in the presence of sodium hydroxide. The preparation of **9** was achieved through the Sonogashira coupling of **8** with (triisopropylsilyl)acetylene (TIPSA). On the other hand, the condensation of **10** with **7** allows the preparation of 9-fluoreneylidene **11**. Compound **12** was readily synthesized from **11** by Vilsmeier–Haack formylation with *N*,*N*-dimethylformamide/$POCl_3$ (DMF/$POCl_3$). Subsequently, **12** was coupled with TIPSA through a Sonogashira reaction to yield **13**. Finally, from the corresponding aldehyde **6**, **9**, or **13**, and cyanoacetic acid in the presence of ammonium acetate and acetic acid as solvent, the target compounds **1**–**3** were prepared in good yields (74–79%) through Knoevenagel condensations.

Photophysical and Electrochemical Properties

The absorption spectra of dyes **1**–**3** in tetrahydrofuran (THF) solution are shown in Figure 2, and the data are listed in Table 1. All of the dyes displayed two major absorption bands; that at $\lambda \approx 350$ nm corresponds to a π–π* transition for the fluorene and bis(ethynyl)fluorene moieties in **1** and **2**–**3**, respectively, and the broad absorption at $\lambda \approx$ 422–460 nm is attributed to an intramolecular charge-transfer (ICT) transition from the triarylamine donor to the cyanoacrylic acid acceptor. The charge-transfer transition should have a lower energy and higher transition probability in conjugated dipolar molecules with stronger donors and acceptors. Among the dyes, compound **3**, which possesses an extra vinyl group between the fluorene and triarylamine groups, displays a redshifted band, which indicates that the donor capability of the triarylamine is improved by the incorporation of the fluorene moiety. Absorption in the longer-wavelength region favors light harvesting by increasing the photocurrent response region.

If dyes **1**–**3** are excited at their λ_{max} absorptions in air-equilibrated solutions at 298 K, they exhibit luminescence maxima at λ = 518 (**1**), 536 (**2**), and 549 (**3**) nm, and the fluorescence quantum yields reveal a more effective quenching process in dye **3** (Figure 2 and Table 1). This fluorescence behavior indicates that the excited state of dye **3** is more stabilized than those of **1** and **2**.

The electrochemical properties of the dyes (Figure 3 and Table 1) were investigated by cyclic voltammetry (CV) and differential pulse voltammetry (DPV) in dichloromethane (DCM) solutions containing 0.1 M tetra-*n*-butylammonium hexafluorophosphate ($TBAPF_6$) as the electrolyte. All of the dyes displayed a quasireversible oxidation wave more positive than the ferrocene (Fc) oxidation potential between +0.57 and +0.69 V versus Fc/Fc^+. Dyes **1** and **3** exhibit a second oxidation wave at 0.79 V, which possibly corresponds to the second oxidation of the triarylamine core. The oxidation potential of dye **3** is the lowest in the series, reflecting the better donor capability of the triarylamine group, in line with the photophysical studies. Under these electrochemical conditions, no reduction processes were observed for the cathodic scans.

The energy level of the highest occupied molecular orbital (HOMO) was estimated from the first oxidation wave relative to the NHE by the conversion $E_{NHE} = (E_{Fc/Fc+} + 0.63\ V)$,[22] as listed in Table 1. The HOMO levels of all dyes were more positive than the reducing potential of the I^-/I_3^- pair (0.4 V vs. NHE);[23] therefore, a sufficient driving force is ensured for the oxidized dyes to recapture an electron from the electrolyte. The lowest unoccupied molecular orbital (LUMO) levels were determined from the first oxidation potential and the 0–0 energy transition (E_{0-0}), estimated from the onset of the normalized absorption spectra. The LUMO levels of all the dyes were higher than the TiO_2 conduction band (–0.5 V vs. NHE);[23] thus, the feasibility of electron injection is ensured (Figure 4).

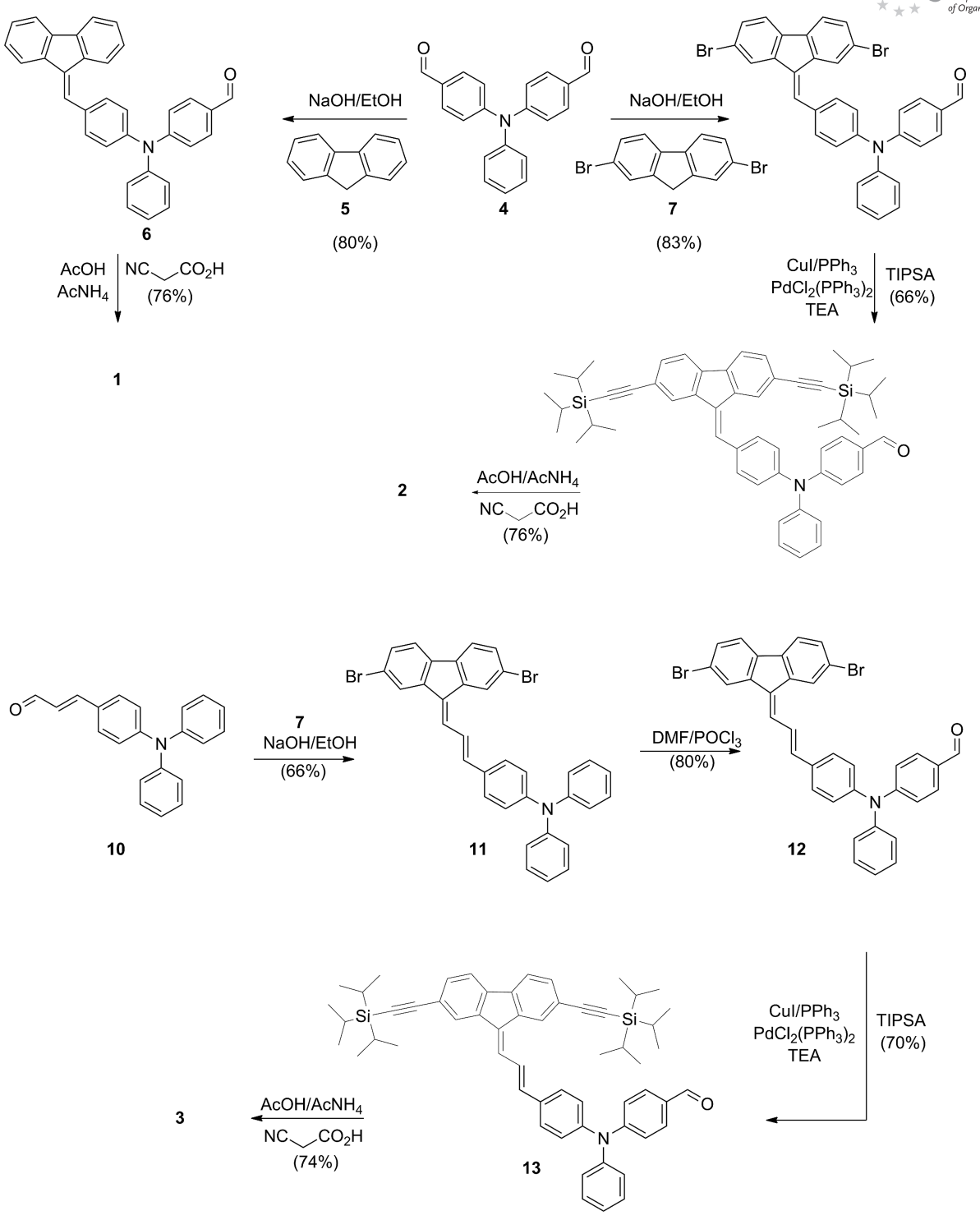

Scheme 1. Synthetic pathways for the preparation of dyes **1**–**3**.

Theoretical Calculations

To analyze the spatial configurations and characteristic features of the electronic structures of the synthesized dyes, molecular geometries and frontier molecular orbitals in the ground and excited states were obtained through DFT and time-dependent DFT (TD-DFT) calculations. The optimized structures of dyes **1**–**3** are shown in Figure 5. The conformations of dyes **1** and **2** represent a structural compromise that minimizes steric hindrance and the π-conjugation pathway, and the dihedral angles between the phenyl rings of the triarylamine moiety and the fluorene moiety are 34 and 36° for **1** and **2**, respectively. As a consequence, the electronic coupling between the fluorene and triarylamine moieties decreases. On the other hand, the additional vinylene spacer in dye **3** allows the π-conjugated junction to adopt a more planar conformation, which leads to better

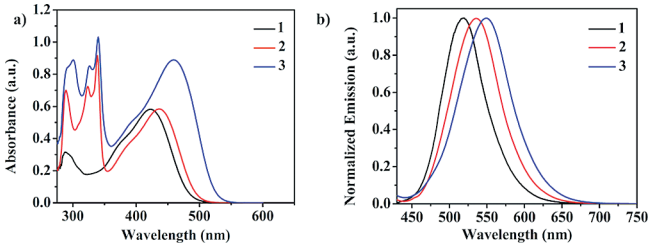

Figure 2. (a) Absorption spectra and (b) normalized fluorescence spectra of dyes **1**–**3** in THF.

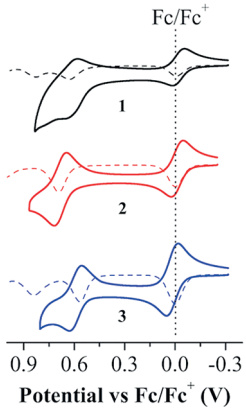

Figure 3. Cyclic voltammetry (solid) and differential pulse voltammetry (dash) of dyes **1**–**3** versus Fc/Fc^+ in $TBAPF_6/CH_2Cl_2$ at a scan rate of 100 mV/s.

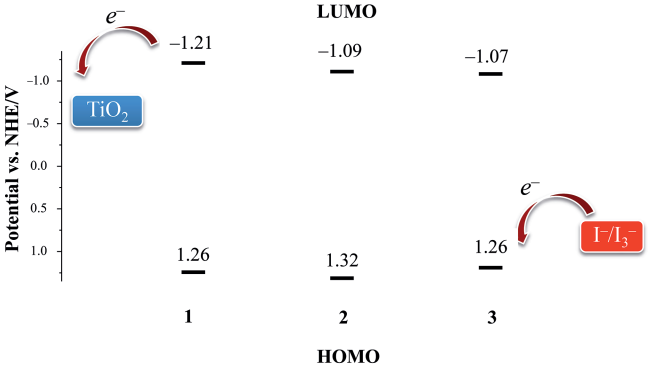

Figure 4. Energy-level diagram of fluorene-9-ylidene dyes **1**–**3**. The redox potential of the iodine couple and the lower edge of the conduction band (CB) of TiO_2 are included for comparison.

electronic coupling. However, both twisted structures and the presence of bulky groups could affect the aggregation and recombination processes and, thus, the overall efficiency of the devices.

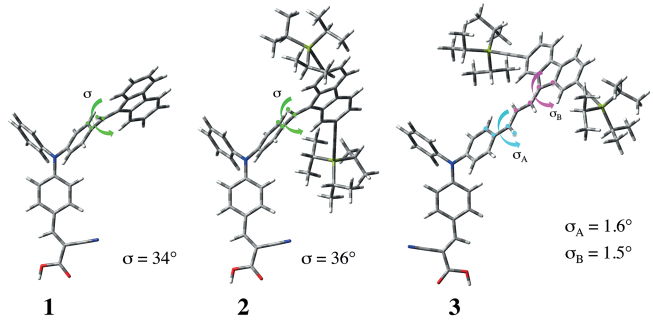

Figure 5. Optimized molecular structures of dyes **1**–**3** calculated with DFT calculations at the B3LYP/6-31G(d) level in vacuo.

The HOMOs of all dyes are localized mainly on the triarylamine and fluorene moieties (particularly in dye **3**), whereas the LUMOs are mainly localized on the cyanoacrylic units with a slight contribution from the fluorene moiety in dyes **1** and **2**, regardless of the presence or absence of the (triisopropylsilyl)acetylene substituent (Figure 6). Thus, the electron distributions are located mainly

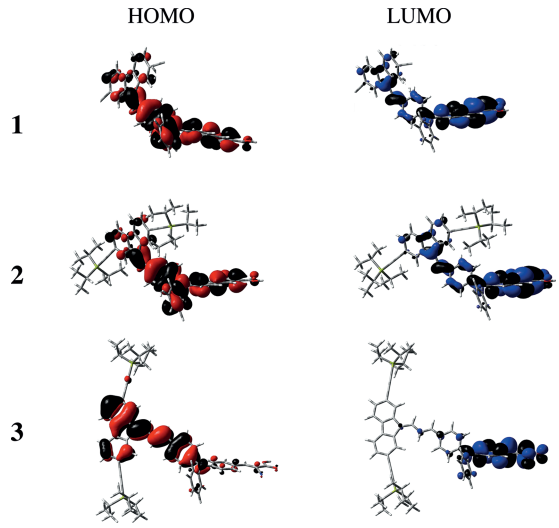

Figure 6. Frontier molecular orbitals (HOMO black-red and LUMO black-blue) of dyes **1**–**3** calculated with DFT at the B3LYP/6-31G(d) level in vacuo.

Table 1. Absorption, emission, and electrochemical characteristics of the studied dyes **1**–**3**.

Dye	λ_{max}[a] [nm] (ε [$M^{-1}cm^{-1}$])	E_{0-0}[b] [nm] (eV)	λ_{em}[c] [nm] (Φ)	E_{ox}[d] [eV] vs. NHE (HOMO)	E_{ox}*[e] [eV] vs. NHE (LUMO)
1	288 (20660), 422 (23280)	501 (2.47)	518 (0.011)	+1.26	–1.21
2	289 (35876), 322 (36880), 338 (46744), 435 (29940)	514 (2.41)	536 (0.010)	+1.32	–1.09
3	300 (38876), 326 (71011), 340 (50012), 460 (67969)	546 (2.27)	549 (0.002)	+1.20	–1.07

[a] Maximum absorption bands in THF (extinction coefficient in $M^{-1}cm^{-1}$). [b] Estimated from the onset of the absorption spectra in THF. [c] Maximum of fluorescence spectra in THF (Φ = quantum yield in THF with Prodan as a reference). [d] Oxidation potential measured vs. Fc^+/Fc in THF converted to normal hydrogen electrode (NHE); $E_{NHE} = (E_{Fc/Fc+} + 0.63)$ V. [e] Estimated by $E_{ox}^* = E_{ox} - E_{0-0}$.

on the donor units in the ground state and are displaced to the acceptor units close to the anchoring groups upon photoexcitation, which favors the electron injection from the dye molecules to the conduction band edge of TiO_2. The particular frontier molecular orbital distribution observed for dye **3** reveals an effective π conjugation across the fluorene–triarylamine junction, as a result of the more planar geometry of **3** than those of dyes **1** and **2**.

The CAM-B3LYP functional and 6-31G(d) basis set were used to calculate the electronic vertical transitions, and solvent effects were included by using the polarizable continuum model (PCM; Table 2). In general, the trends in the excitation energies are consistent with the solution spectroscopic data in THF. The results suggest that the longer-wavelength absorptions correspond to the HOMO-to-LUMO vertical excitation in all cases. As the HOMOs of the dyes are mainly localized on the triarylamine group, and the LUMO spreads over the phenyl ring of the triarylamine moiety and the cyanoacrylic acid, it can be argued that the longer-wavelength absorptions result from charge-transfer processes for all of the dyes.

Table 2. Computed vertical transition energies and their oscillator strengths and configurations for the dyes **1**–**3**.

Functional	Parameter	**1**	**2**	**3**
CAM-B3LYP (THF)	λ_{max} [nm]	414	423	452
	f	4.1793	7.6788	4.1399
	Configuration (Contribution)	H→L (0.87)	H→L (0.93)	H→L (0.69)
	HOMO [eV]	–5.33	–5.46	–5.17
	LUMO [eV]	–1.86	–2.42	–3.10

Photovoltaic Performance of DSSCs of 1–3

The preparation of the DSSC devices is described in the Experimental Section. For sensitization, the films were impregnated with 0.3 mM solution of dyes **1**–**3** in THF for 4 h at room temperature. The samples were then rinsed with the same solvent to remove unadsorbed dyes from the surface of the photoelectrodes and air-dried at room temperature. This was followed by the addition of the redox electrolyte and the top contact of Pt-coated fluorine-doped tin oxide (FTO). The *J*–*V* characteristics were measured by using a solar simulator at approximately 100 mW/cm^2.

The device performances are summarized in Table 3, and the optimal results are shown in Figure 7. The devices fabricated with dyes **1**–**3** gave overall conversion efficiencies (η) of 3.98, 4.09, and 4.73%, respectively. The efficiency of dye **3** reached more than 60% of the efficiency of devices made with the standard N719 complex (η = 7.30%) under the same conditions.

Table 3. Performance parameters of the DSSCs fabricated with dyes **1**–**3** and N719.

Dye	V_{oc} [V]	J_{sc} [mA/cm^2]	FF	η[a] [%]
1	0.79	6.84	0.75	3.98
2	0.83	6.63	0.74	4.09
3	0.81	9.59	0.62	4.73
N719	0.80	17.6	0.55	7.42

[a] Best cell efficiency.

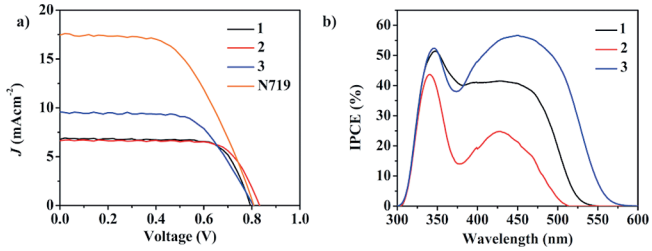

Figure 7. (a) *I*–*V* characteristics of the DSSCs fabricated with dyes **1**–**3** and N719, (b) IPCE spectra of the DSSCs fabricated with dyes **1**–**3**.

The molecular structures of dyes **1**–**3** differ only by an additional TIPSA group between **1** and **2** and by an internal additional vinyl group between **2** and **3**. These relatively minor modifications have a significant impact on the photovoltaic performances. Dyes **1** and **2** show very similar fill factors (FF), whereas the FF value for dye **3** decreases by 17%. The broadening of the incident photon conversion efficiency (IPCE) spectra is desired to obtain larger photocurrents (short-circuit current density, J_{sc}).[24] The dyes exhibit maximum IPCE (>50%) between 340 and 500 nm, and the IPCE spectra broaden and extend to 580 nm on the incorporation of an additional vinyl unit (for instance, compare **3** with **1** or **2**), which is consistent with the bathochromic shift observed for this dye in solution and loaded TiO_2 films (Figure 7). These observations explain the higher J_{sc} exhibited by dye **3**.

Concerning the open-cell voltage (V_{oc}) properties, it was noticed that the introduction of TIPSA groups improved the photovoltages for these dyes, possibly by decreasing the dark current generated by reduction of I_3^- with the injected electrons owing to the occurrence of sterically highly hindered groups on the TiO_2 surface, as reported previously for organometallic complexes[19] and metal-free chromophores.[18] Noticeably, the V_{oc} of dye **3** is higher than the voltage of devices made with N719 complex.

Electrochemical Impedance Spectroscopy

The charge recombination at the TiO_2/electrolyte interface was investigated by electrochemical impedance spectroscopy (EIS), which is a versatile steady-state method to elucidate the electronic and ionic processes occurring in DSSCs. Typical EIS Nyquist plots for DSSCs based on the three dyes measured under illumination and in the dark under a forward bias of –0.80 V are shown in Figures 8 and S10.

Bulky alkyl and aryl groups in organic dyes are reported to enhance electron lifetimes by blocking the redox species from approaching the TiO_2 electrode.[17] For dyes **1**–**3**, the fluorene groups in the triarylamine core are expected to exert similar blocking effects. A standard equivalent circuit model for DSSCs consisting of a series resistance (R_S) and

charge-transfer resistances (R_{CT}) in series, constant-phase elements (CPEs), and a Warburg diffusion constant (W) was used to satisfactorily model the impedance experimental data (Figure 8, inset). The CPEs were introduced in the equivalent circuit model instead of chemical capacitances (C) to compensate for inhomogeneities and the porosity of the TiO_2.[25] The experimentally extracted parameters from the fitted impedance spectra under illumination are summarized in Table S1. The fitted interfacial charge-transfer resistances (R_{CT}) for TiO_2/dye/electrolyte vary from one dye to another in the sequence **3** (182 Ω) > **2** (104 Ω) > **1** (98 Ω; see Table S1), which indicates that the recombination of conduction band electrons with the electrolyte is more difficult for highly bulky dyes. When comparing dye **1** with **2** and **3**, we noticed a dramatic increase of the R_{CT} values, which is attributed to the presence of the bulky (triisopropylsilyl)acetylene groups. On the other hand, it was expected that planarity would increase with the expansion of π conjugation between the fluorene and triarylamine groups. These geometrical variations could minimize the blocking effect of the antenna and, therefore, the differences in the V_{oc} values.

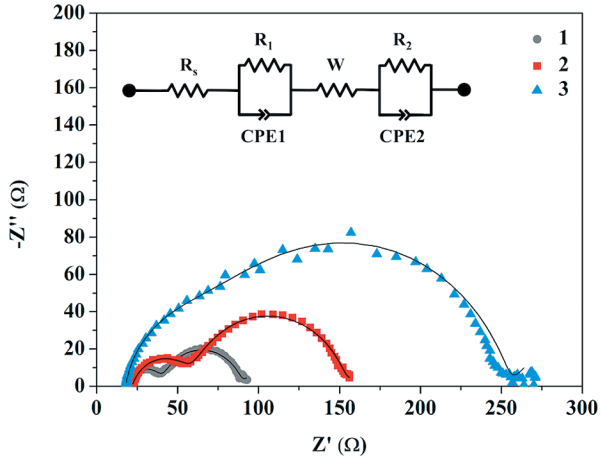

Figure 8. Nyquist plots of the impedance data of DSSCs with **1**–**3** under illumination. The solid lines represent the modeled impedance data.

The effective electron lifetimes can be estimated from the electrochemical impedance data by using the equation $\tau_{eff} = 1/2\pi f_{max}$, in which $f_{max} = f(-Z'')_{max}$.[26] The f_{max} values for the DSSCs under illumination are 11.19, 6.64, and 147 Hz for **1**–**3**, respectively (see Table S2). Consequently, the estimated electron lifetimes follow the trend **2** (2.40 ms) > **1** (1.47 ms) > **3** (0.108 ms). Despite the faster charge-carrier recombination rate of **3**, represented by the lower electron lifetime, a higher overall device performance was achieved. This is attributed to contributions from the TIPSA bulky groups and the incorporation of an additional vinylene unit, which results in a wider absorption spectrum for **3** than those of **1** and **2**.

Conclusions

We have synthesized three new dyes based on triarylamine donors with different fluorene-9-ylidene groups as antennas and cyanoacrylic acid acceptors. The compounds were fully characterized by optoelectronic techniques.

The electrochemical and photophysical measurements predicted the feasibility of electron injection into the conducting band of TiO_2 and dye regeneration by the electrolyte. Devices were constructed, and their photovoltaic performances were evaluated. The η values followed the trend **3** (4.73%) > **2** (4.09%) > **1** (3.98%); an N719 reference cell has a value of 7.42% under the same conditions.

Owing to the incorporation of the fluorene-9-ylidene unit into the dye skeleton, a V_{oc} as high as 0.794 V was observed. Additional improvements were achieved through the introduction of highly hindered groups such as TIPSA, and a V_{oc} value of 0.832 V was achieved. Furthermore, the introduction of the bulky TIPSA group resulted in overall device efficiency increases of 3 and 18.8% for **2** and **3**, respectively. Therefore, the additional vinyl unit connecting the fluorene-9-ylidene and triarylamine groups within the framework of **3** expanded the π-conjugation length of the dye, which resulted in wider absorption in the visible region and consequently enhanced the IPCE and resulted in an overall efficiency of 4.73%.

Experimental Section

Materials and Instrument Measurements: Reagents were used as purchased unless stated otherwise. Compounds **4** and **10** were prepared according to literature procedures. All solvents were dried according to standard procedures. All air-sensitive reactions were conducted under argon. FTIR spectra were recorded with a Shimadzu FTIR 8400 spectrometer. Absorption studies were performed with a Varian Cary 5000 UV/Vis/NIR spectrometer with samples in fused quartz cuvettes with a 1 cm optical path. Fluorescence measurements were performed with a JASCO spectrofluorometer (FP-8500). NMR spectra were recorded with a 400 MHz Bruker (^{1}H: 400 MHz; ^{13}C: 100 MHz) spectrometer at 298 K by using partially deuterated solvents as internal standards. Coupling constants (J) are reported in Hz, and chemical shifts (δ) are reported in ppm. Multiplicities are denoted as follows: s = singlet, d = doublet, t = triplet, m = multiplet, dd = doublet of doublets. Mass spectra were recorded with a Shimadzu MS-QP 2010 spectrometer operating at 70 eV or a Bruker microFLEX LRF MALDI-TOF spectrometer. Analytical thin layer chromatography (TLC) was performed with aluminum-coated Sorbent technologies 60 UV254 plates.

Electrochemical Measurements: All electrochemical measurements were conducted in anhydrous dichloromethane (Acros, 99.9%) under argon by using a CHI440B electrochemical workstation (CH Instruments, Inc.). Tetrabutylammonium hexafluorophosphate (Aldrich, 98%) was recrystallized from ethanol and added as the supporting electrolyte (0.10 M). A three-electrode configuration consisting of a 1.0 mm glassy carbon working electrode, a platinum wire counter electrode (Aldrich, 1.0 mm), and a silver wire pseudoreference electrode (Aldrich, 1.0 mm) was used. The ferrocene/ferrocenium (Fc/Fc^+) redox couple was used as the internal reference to measure the potentials. All potentials were further converted into values relative to the normal hydrogen electrode (NHE) by $E_{NHE} = (E_{Fc/Fc+} + 0.63)$ V. Electrochemical impedance spectroscopy (EIS) results were obtained with a CHI660A electrochemical workstation (CH Instruments) in the frequency range 1.0×10^5 to 0.1 Hz with an alternating current (AC) amplitude of 5 mV. The

working electrode was connected to the TiO_2 electrode, and the counter and reference electrode were connected to the Pt counter electrode. The obtained spectra were fitted to an equivalent circuit (Figure 8, inset) with the EIS Spectrum Analyzer software.[27]

DSSC Fabrication: FTO-coated glass slide sheets (Aldrich, 300 × 300 × 2 mm, 7 Ω/sq) were cut into 2 × 2 cm squares. The FTO slides were sonicated in Alconox® detergent solution for 20 min, rinsed with deionized (DI) water, and then sonicated in DI water and ethanol for 20 min each. The slides were dried with a flow of N_2 gas and UV-treated in a UV/ozone 342 apparatus (Jelight Co.) for 18 min. The FTO slides were then treated with a 40 mM $TiCl_4$ aqueous solution at 70 °C for 30 min. The semiconductor TiO_2, electrolyte, and Pt counter electrodes were prepared as reported previously.[28] Solutions (0.3 mM) of dyes **1**–**3** were prepared in THF, and the TiO_2 substrates were submerged in each solution for 4 h. After this time, the substrates were rinsed with fresh THF to remove unadsorbed dyes. To prepare the DSSC devices, a tape gasket was used to load the electrolyte, and the cell was backed with the Pt counter electrode. All cell areas were 0.25 cm^2, and they were tested at 1.5 AM (Air Mass) by using a Photo Emission Tech SS100 Solar Simulator at approximately 100 mW/cm^2 irradiance.

4-[{4-[(9*H*-Fluoren-9-ylidene)methyl]phenyl}(phenyl)amino]benzaldehyde (6): A solution of 4,4′-(phenylazanediyl)dibenzaldehyde (**4**; 151 mg, 0.5 mmol), fluorene (**5**; 83 mg, 0.5 mmol), and NaOH (1.0 mL, 20% in water) in ethanol (20 mL) was heated at reflux for 5 h. After evaporation of the solvent, the crude product was purified by SiO_2 flash column chromatography with hexane/DCM (1:1) as the eluent to yield **6** (180 mg, 80%) as a yellow solid; m.p 169 °C. IR: $\tilde{\nu}$ = 1689, 1580, 1511 cm^{-1}. ^1H NMR (400 MHz, $CDCl_3$, 298 K): δ = 9.88 (s, 1 H), 7.83 (d, J = 7.8 Hz, 1 H), 7.83–7.80 (m, 5 H), 7.65 (s, 1 H), 7.61 (d, J = 8.5 Hz, 1 H), 7.47–7.32 (m, 6 H), 7.31–7.23 (m, 2 H), 7.23–7.19 (m, 3 H), 7.18 (d, J = 8.5 Hz, 2 H) ppm. ^{13}C NMR (100 MHz, $CDCl_3$, 298 K): δ = 190.5, 153.1, 146.1, 141.4, 139.6, 139.1, 136.5, 136.3, 133.0, 131.4, 131.0, 130.0, 129.8, 128.7, 128.2, 127.1, 126.7, 126.6, 126.5, 126.4, 125.5, 125.3, 124.3, 120.4, 120.2, 119.9, 119.7 ppm. MS (EI): m/z = 449.2 $[M]^+$. $C_{33}H_{23}NO$ (449.55): calcd. C 88.17, H 5.16, N 3.12; found C 88.54, H 5.36, N 3.02.

4-[{4-[(2,7-Dibromo-9*H*-fluoren-9-ylidene)methyl]phenyl}(phenyl)amino]benzaldehyde (8): A solution of 4,4′-(phenylazanediyl)dibenzaldehyde (**4**; 301 mg, 1.0 mmol), 2,7-dibromofluorene (348 mg, 1.0 mmol), and NaOH (1.0 mL, 20% in water) in ethanol (20 mL) was heated at reflux for 5 h. After evaporation of the solvent, the crude product was purified by SiO_2 flash column chromatography with hexane/DCM (2:1) as the eluent to yield **8** (500 mg, 83%) as an orange solid; m.p 120–122 °C. IR: $\tilde{\nu}$ = 1691, 1588, 1503 cm^{-1}. ^1H NMR (400 MHz, $CDCl_3$, 298 K): δ = 9.87 (s, 1 H), 7.88 (d, J = 1.2 Hz, 1 H), 7.76 (d, J = 8.8 Hz, 2 H), 7.71 (d, J = 1.8 Hz, 1 H), 7.66 (s, 1 H), 7.54 (d, J = 8.0 Hz, 2 H), 7.52–7.47 (m, 3 H), 7.46 (dd, J = 1.8, J = 8.2 Hz, 1 H), 7.41 (t, J = 7.9 Hz, 2 H), 7.30–7.21 (m, 6 H), 7.19 (d, J = 8.8 Hz, 2 H) ppm. ^{13}C NMR (100 MHz, $CDCl_3$, 298 K): δ = 190.5, 152.9, 146.9, 146.0, 141.0, 139.1, 138.1, 136.9, 134.6, 131.8, 131.3, 131.4, 131.2, 130.7, 130.0, 129.9, 129.3, 127.5, 126.5, 125.5, 125.3, 123.7, 121.3, 121.1, 121.0, 120.7 ppm. MS (EI) m/z = 605.0 $[M]^+$. $C_{33}H_{21}Br_2NO$ (607.35): calcd. C 65.26, H 3.49, N 2.31; found C 65.74, H 3.57, N 2.51.

4-{[4-({2,7-Bis[(triisopropylsilyl)ethynyl]-9*H*-fluoren-9-ylidene}methyl)phenyl](phenyl)amino}benzaldehyde (9): A solution of **8** (400.0 mg, 0.66 mmol), $Pd(PPh_3)Cl_2$ (35.1 mg, 0.05 mmol), CuI (19.0 mg, 0.1 mmol), PPh_3 (26.2 mg, 0.1 mmol), and TIPSA (273 mg, 1.5 mmol) in dry triethylamine (TEA; 15.0 mL) was heated under reflux for 12 h. After evaporation of the solvent, the crude product was purified by SiO_2 flash column chromatography with hexane/DCM (2:1) as the eluent to yield **9** (394 mg, 66%) as a yellow solid; m.p 106–107 °C. IR: $\tilde{\nu}$ = 2942, 2863, 2151, 1695 cm^{-1}. ^1H NMR (400 MHz, $CDCl_3$, 298 K): δ = 9.87 (s, 1 H), 8.04, (s, 1 H), 7.88 (s, 1 H), 7.75 (d, J = 8.8 Hz, 2 H), 7.67 (s, 1 H), 7.66 (d, J = 3.1 Hz, 1 H), 7.64 (d, J = 3.1 Hz, 1 H), 7.61 (d, J = 8.4 Hz, 2 H), 7.51 (dd, J = 7.8, J = 1.2 Hz, 1 H), 7.47 (dd, J = 7.8, J = 1.2 Hz, 1 H), 7.40 (t, J = 7.9 Hz, 2 H), 7.26–7.20 (m, 5 H), 7.16 (d, J = 8.8 Hz, 2 H), 1.18 (s, 21 H), 1.10 (s, 21 H) ppm. ^{13}C NMR (100 MHz, $CDCl_3$, 298 K): δ = 190.5, 153.0, 146.6, 146.1, 140.5, 139.9, 138.3, 136.6, 136.4, 134.6, 132.2, 132.1, 131.9, 131.4, 131.0, 130.0, 129.9, 128.3, 128.1, 126.7, 125.5, 124.8, 123.9, 122.3, 121.9, 120.8, 119.9, 119.7, 107.8, 107.7, 91.0, 90.8, 18.8, 11.4, 11.3 ppm. HRMS (MALDI-TOF): calcd. for $C_{55}H_{63}NOSi_2$ $[M]^+$ 809.4448; found 809.6302. $C_{55}H_{63}NOSi_2$ (810.29): calcd. C 81.53, H 7.84, N 1.73; found C 81.59, H 7.98, N 1.79.

(*E*)-4-[3-(2,7-Dibromo-9*H*-fluoren-9-ylidene)prop-1-en-1-yl]-*N*,*N*-diphenylaniline (11): A solution of (*E*)-3-[4-(diphenylamino)phenyl]acrylaldehyde (**10**; 150 mg, 0.50 mmol), 2,7-dibromofluorene (162 mg, 0.50 mmol), and NaOH (10.0 mL, 20% in water) in ethanol (20.0 mL) was heated to reflux for 10 h. After evaporation of the solvent, the crude product was purified by SiO_2 column chromatography with hexane/DCM (7:1) as the eluent to yield **11** (200 mg, 66%) as an orange solid; m.p 100–101 °C. IR: $\tilde{\nu}$ = 2942, 1600, 1525 cm^{-1}. ^1H NMR (400 MHz, $CDCl_3$, 298 K): δ = 8.11 (s, 1 H), 7.84 (d, J = 1.4 Hz, 1 H), 7.69 (t, J = 14.0 Hz, 1 H), 7.60 (d, J = 8.0 Hz, 1 H), 7.55 (d, J = 8.0 Hz, 1 H), 7.51–7.42 (m, 4 H), 7.36–7.28 (m, 5 H), 7.17 (d, J = 7.6 Hz, 4 H), 7.14–7.06 (m, 4 H), 7.02 (d, J = 14.0 Hz, 1 H) ppm. ^{13}C NMR (100 MHz, $CDCl_3$, 298 K): δ = 147.1, 141.4, 141.1, 138.8, 138.4, 136.4, 131.3, 130.4, 130.3. 130.2, 129.8, 129.5, 128.5, 127.9, 125.3, 125.2, 123.9, 123.2, 122.4, 121.9, 121.2, 121.1, 120.9, 120.8 ppm. MS (EI): m/z = 603.0 $[M]^+$. $C_{34}H_{23}Br_2N$ (605.37): calcd. C 67.46, H 3.83, N 2.31; found C 67.70, H 3.93, N 2.39.

(*E*)-4-[{4-[3-(2,7-Dibromo-9*H*-fluoren-9-ylidene)prop-1-en-1-yl]phenyl}(phenyl)amino]benzaldehyde (12): A solution of **11** (150 mg, 0.25 mmol) and $POCl_3$ (153.0 mg, 1.0 mmol) in DMF (3.0 mL) was heated at 80 °C for 48 h. Then, water (30 mL) was added to quench the reaction, the solution was neutralized with K_2CO_3, and the aqueous phase was extracted with DCM (3 × 20 mL). After evaporation of the solvent, the crude product was purified by SiO_2 column chromatography with DCM as the eluent to yield **12** (126 mg, 80%) as a red solid; m.p 128–130 °C. IR: $\tilde{\nu}$ = 2970, 1690, 1530 cm^{-1}. ^1H NMR (400 MHz, $CDCl_3$, 298 K): δ = 9.87 (s, 1 H), 8.10 (d, J = 1.6 Hz, 1 H), 7.83 (d, J = 1.6 Hz, 1 H), 7.78–7.68 (m, 3 H), 7.59 (d, J = 8.6 Hz, 1 H), 7.57–7.51 (m, 3 H), 7.49 (dd, J = 8.1, J = 1.6 Hz, 1 H), 7.45 (dd, J = 8.1, J = 1.6 Hz, 1 H), 7.39 (t, J = 7.5 Hz, 2 H), 7.32 (d, J = 11.9 Hz, 1 H), 7.26–7.18 (m, 5 H), 7.14 (d, J = 8.6 Hz, 2 H), 7.03 (d, J = 15.2 Hz, 1 H) ppm. ^{13}C NMR (100 MHz, $CDCl_3$, 298 K): δ = 190.5, 152.8, 147.2, 145.9, 141.3, 140.2, 138.7, 138.6, 136.6, 132.5, 132.3, 131.4, 130.7, 130.6, 130.1, 130.0, 129.7, 128.7, 128.0, 126.6, 125.6, 125.3, 123.4, 123.3, 121.3, 121.2, 121.0, 120.9, 120.8 ppm. MS (EI): m/z = 631.0 $[M]^+$. $C_{35}H_{23}Br_2NO$ (633.38): calcd. C 66.37, H 3.66, N 2.21; found C 66.67, H 3.70, N 2.67.

(*E*)-4-{[4-(3-{2,7-Bis[(triisopropylsilyl)ethynyl]-9*H*-fluoren-9-ylidene}prop-1-en-1-yl)phenyl](phenyl)amino}benzaldehyde (13): A solution of **12** (110.0 mg, 0.17 mmol), $Pd(PPh_3)Cl_2$ (35.2 mg, 0.05 mmol), CuI (19.0 mg, 0.1 mmol), PPh_3 (26.0 mg, 0.1 mmol), and TIPSA (100 mg, 0.55 mmol) in dry TEA (10.0 mL) was heated at 70 °C for 20 h. After evaporation of the solvent, the crude product was purified by SiO_2 column chromatography with hexane/

DCM (3:1) as the eluent to yield **13** (100 mg, 70%) as an orange solid; m.p 90–92 °C. IR: $\tilde{\nu}$ = 2990, 2148, 1692 cm^{-1}. ^1H NMR (400 MHz, $CDCl_3$, 298 K): δ = 9.87 (s, 1 H), 8.17 (s, 1 H), 7.91 (dd, J = 1.2, J = 15.0 Hz, 1 H), 7.84 (s, 1 H), 7.75 (d, J = 8.8 Hz, 2 H), 7.68 (d, J = 7.8 Hz, 1 H), 7.63 (d, J = 7.8 Hz, 1 H), 7.54 (d, J = 8.8 Hz, 2 H), 7.48 (t, J = 8.4 Hz, 3 H), 7.43–7.35 (m, 3 H), 7.26–7.19 (m, 3 H), 7.15 (t, J = 9.0 Hz, 4 H), 7.03 (d, J = 15.0 Hz, 1 H), 1.19 (s, 21 H), 1.16 (s, 21 H) ppm. ^{13}C NMR (100 MHz, $CDCl_3$, 298 K): δ = 190.5, 152.8, 146.8, 145.9, 140.0, 139.8, 138.7, 138.1, 137.5, 133.4, 133.1, 131.7, 131.4, 131.3, 129.9, 129.1, 128.6, 128.4, 126.6, 125.6, 125.4, 124.2, 123.8, 122.2, 122.1, 120.6, 120.1, 119.8, 108.0, 107.8, 91.2, 90.9, 68.1, 18.8, 18.7, 11.5, 11.4 ppm. HRMS (MALDI-TOF): calcd. for $C_{57}H_{65}NOSi_2$ 835.4605; found 835.4009. $C_{57}H_{65}NOSi_2$ (836.32): calcd. C 81.86, H 7.83, N 1.67; found C 81.90, H 7.84, N 1.76.

General Procedure for the Preparation of Dyes 1–3: The corresponding aldehyde (0.1 mmol), cyanoacetic acid (0.4 mmol), and ammonium acetate (1.0 mmol) were dissolved in acetic acid (10 mL), and the mixture was heated under reflux for 4 h. After cooling to room temperature, the mixture was poured into ice/water. The resulting precipitate was collected by filtration and washed with water. The solid was dissolved in DCM and washed with brine. The organic phase was dried with anhydrous $MgSO_4$, and the solvent was removed under reduced pressure. The crude product was purified by column chromatography (silica gel) with methanol/dichloromethane (1:30) as the eluent.

(*E*)-2-Cyano-3-{4-[{4-[(9*H*-fluoren-9-ylidene)methyl]phenyl}(phenyl)amino]phenyl}acrylic Acid (1): Orange solid, 76%; m.p 128 °C. IR: $\tilde{\nu}$ = 3410, 2221, 1687 cm^{-1}. ^1H NMR (400 MHz, $CDCl_3$, 298 K): δ = 8.15 (s, 1 H), 7.84 (d, J = 8.2 Hz, 2 H), 7.76–7.65 (m, 4 H), 7.55 (s, 1 H), 7.51 (d, J = 8.0 Hz, 2 H), 7.38–7.28 (m, 4 H), 7.20–7.07 (m, 6 H), 7.05–6.98 (m, 3 H) ppm. ^{13}C NMR (100 MHz, $CDCl_3$, 298 K): δ = 151.6, 145.6, 145.5, 141.3, 139.6, 139.1, 136.4, 136.2, 135.8, 133.3, 131.0, 130.0, 128.6, 128.3, 128.2, 127.0, 126.8, 126.7, 126.4, 125.7, 125.6, 125.3, 124.2, 120.2, 120.1, 119.8, 119.6 ppm. MS (EI): m/z = 516.2 $[M]^+$. $C_{36}H_{24}N_2O_2$ (516.60): calcd. C 83.70, H 4.68, N 5.42; found C 83.76, H 4.77, N 5.47.

3-(4-{[4-({2,7-Bis[(triisopropylsilyl)ethynyl]-9*H*-fluoren-9-ylidene}methyl)phenyl](phenyl)amino}phenyl)-2-cyanoacrylic Acid (2): Red solid, 79%; m.p 213 °C. IR: $\tilde{\nu}$ = 3424, 2940, 2220, 2150, 1692, 1577 cm^{-1}. ^1H NMR (400 MHz, $CDCl_3$, 298 K): δ = 8.17 (s, 1 H), 8.01 (s, 1 H), 7.94 (d, J = 9.2 Hz, 2 H), 7.88 (s, 1 H), 7.68 (s, 1 H), 7.67–7.61 (m, 4 H), 7.51 (dd, J = 7.8, J = 1.2 Hz, 1 H), 7.46 (dd, J = 7.8, J = 1.2 Hz, 1 H), 7.42 (t, J = 7.8 Hz, 2 H), 7.30–7.22 (m, 5 H), 7.11 (d, J = 9.2 Hz, 2 H), 1.18 (s, 21 H), 1.10 (s, 21 H) ppm. ^{13}C NMR (100 MHz, $CDCl_3$, 298 K): δ = 167.6, 155.3, 152.6, 145.9, 145.5, 140.6, 139.8, 136.6, 134.9, 133.6, 132.7, 132.3, 131.1, 130.1, 128.2, 128.1, 126.8, 126.1, 125.3, 123.9, 122.4, 121.9, 121.1, 120.2, 119.9, 116.2, 107.8, 107.6, 107.4, 96.7, 91.1, 90.8, 18.8, 11.4, 11.3 ppm. MS (EI): m/z = 876.5 $[M]^+$. $C_{58}H_{64}N_2O_2Si_2$ (877.33): C 79.40, H 7.35, N 3.19; found C 79.55, H 7.39, N 3.40.

(*E*)-3-{4-[{4-[(*E*)-3-{2,7-Bis[(triisopropylsilyl)ethynyl]-9*H*-fluoren-9-ylidene}prop-1-en-1-yl]phenyl}(phenyl)amino]phenyl}-2-cyanoacrylic Acid (3): Red solid, 74%; m.p 70 °C. IR: $\tilde{\nu}$ = 3423, 2890, 2221, 2149, 1684 cm^{-1}. ^1H NMR (400 MHz, $CDCl_3$, 298 K): δ = 8.16 (s, 2 H), 7.96–7.87 (m, 3 H), 7.84 (s, 1 H), 7.68 (d, J = 7.6 Hz, 1 H), 7.63 (d, J = 7.8 Hz, 1 H), 7.55 (d, J = 8.6 Hz, 2 H), 7.52–7.45 (m, 2 H), 7.45–7.36 (m, 3 H), 7.23 (d, J = 7.6 Hz, 2 H), 7.18 (d, J = 8.6 Hz, 2 H), 7.12–7.05 (m, 3 H), 7.01 (d, J = 12.9 Hz, 1 H), 1.18 (s, 21 H), 1.15 (s, 21 H) ppm. ^{13}C NMR (100 MHz, $CDCl_3$, 298 K): δ = 152.5, 145.4, 144.0, 140.1, 139.8, 138.6, 137.5, 133.7, 133.6, 131.8, 131.5, 130.1, 128.6, 128.5, 126.9, 126.2, 126.0, 125.6, 124.6, 123.9, 122.3, 122.2, 120.2, 120.0, 119.9, 108.0, 107.8, 107.5, 18.9, 18.8, 11.5, 11.4 ppm. HRMS (MALDI-TOF): calcd. for $C_{60}H_{66}N_2O_2Si_2$ $[M]^+$ 902.4663; found 902.4600. $C_{60}H_{66}N_2O_2Si_2$ (903.37): calcd. C 79.77, H 7.36, N 3.10; found C 80.01, H 7.46, N 3.22%.

Acknowledgments

The authors wish to thank Universidad del Valle, COLCIENCIAS, the US Air Force Office of Scientific Research (Grants FA9550-12-1-0053 and FA9550-12-1-0468), the NSF Partnership for Research and Education in Materials (DMR-1205302), and the Robert A. Welch Foundation (AH-0033) for generous support for this work. The authors would like to thank Robert Cotta for technical advice in the preparation of DSSCs.

[1] J.-L. Bredas, J. R. Durrant, *Acc. Chem. Res.* **2009**, *42*, 1689–1690.
[2] a) B. O'Regan, M. Grätzel, *Nature* **1991**, *353*, 737–740; b) S. Zhang, X. Yang, Y. Numata, L. Han, *Energy Environ. Sci.* **2013**, *6*, 1443–1464; c) M. Grätzel, *Acc. Chem. Res.* **2009**, *42*, 1788–1798.
[3] H. Imahori, T. Umeyama, S. Ito, *Acc. Chem. Res.* **2009**, *42*, 1809–1818.
[4] L. M. Peter, *J. Phys. Chem. Lett.* **2011**, *2*, 1861–1867.
[5] M. Grätzel, *Inorg. Chem.* **2005**, *44*, 6841–6851.
[6] a) A. Yella, H.-W. Lee, H. N. Tsao, C. Yi, A. K. Chandiran, M. K. Nazeeruddin, E. W.-G. Diau, C.-Y. Yeh, S. M. Zakeeruddin, M. Grätzel, *Science* **2011**, *334*, 629–634; b) A. Yella, C.-L. Mai, S. M. Zakeeruddin, S.-N. Chang, C.-H. Hsieh, C.-Y. Yeh, M. Grätzel, *Angew. Chem. Int. Ed.* **2014**, *53*, 2973–2977; *Angew. Chem.* **2014**, *126*, 3017–3021; c) L.-L. Li, E. W.-G. Diau, *Chem. Soc. Rev.* **2013**, *42*, 291–304.
[7] J.-H. Yum, E. Baranoff, S. Wenger, M. K. Nazeeruddin, M. Grätzel, *Energy Environ. Sci.* **2011**, *4*, 842–857.
[8] a) A. Hagfeldt, G. Boschloo, L. Sun, L. Kloo, H. Pettersson, *Chem. Rev.* **2010**, *110*, 6595–6663; b) Z. Ning, H. Tian, *Chem. Commun.* **2009**, 5483–5495; c) J. N. Clifford, E. Martinez-Ferrero, A. Viterisi, E. Palomares, *Chem. Soc. Rev.* **2011**, *40*, 1635–1646.
[9] K. Hara, T. Sato, R. Katoh, A. Furube, Y. Ohga, A. Shinpo, S. Suga, K. Sayama, H. Sugihara, H. Arakawa, *J. Phys. Chem. B* **2002**, *107*, 597–606.
[10] B. Liu, Q. Liu, D. You, X. Li, Y. Naruta, W. Zhu, *J. Mater. Chem.* **2012**, *22*, 13348–13356.
[11] a) C. A. Echeverry, A. Insuasty, M. Á. Herranz, A. Ortíz, R. Cotta, V. Dhas, L. Echegoyen, B. Insuasty, N. Martín, *Dyes Pigm.* **2014**, *107*, 9–14; b) D. Arteaga, R. Cotta, A. Ortiz, B. Insuasty, N. Martin, L. Echegoyen, *Dyes Pigm.* **2015**, *112*, 127–137.
[12] W. Zeng, Y. Cao, Y. Bai, Y. Wang, Y. Shi, M. Zhang, F. Wang, C. Pan, P. Wang, *Chem. Mater.* **2010**, *22*, 1915–1925.
[13] a) Y. Ooyama, Y. Harima, *ChemPhysChem* **2012**, *13*, 4032–4080; b) D. P. Hagberg, J.-H. Yum, H. Lee, F. De Angelis, T. Marinado, K. M. Karlsson, R. Humphry-Baker, L. Sun, A. Hagfeldt, M. Grätzel, M. K. Nazeeruddin, *J. Am. Chem. Soc.* **2008**, *130*, 6259–6266; c) B. Lim, G. Y. Margulis, J.-H. Yum, E. L. Unger, B. E. Hardin, M. Grätzel, M. D. McGehee, A. Sellinger, *Org. Lett.* **2013**, *15*, 784–787.
[14] G. Boschloo, L. Häggman, A. Hagfeldt, *J. Phys. Chem. B* **2006**, *110*, 13144–13150.
[15] A. Kay, M. Grätzel, *J. Phys. Chem.* **1993**, *97*, 6272–6277.
[16] Y. Numata, A. Islam, H. Chen, L. Han, *Energy Environ. Sci.* **2012**, *5*, 8548–8552.
[17] J. E. Kroeze, N. Hirata, S. Koops, M. K. Nazeeruddin, L. Schmidt-Mende, M. Grätzel, J. R. Durrant, *J. Am. Chem. Soc.* **2006**, *128*, 16376–16383.

[18] G. Marzari, J. Durantini, D. Minudri, M. Gervaldo, L. Otero, F. Fungo, G. Pozzi, M. Cavazzini, S. Orlandi, S. Quici, *J. Phys. Chem. C* **2012**, *116*, 21190–21200.
[19] J. Xu, H. Wu, X. Jia, D. Zou, *Chem. Commun.* **2012**, *48*, 7793–7795.
[20] C. Du, C. Li, W. Li, X. Chen, Z. Bo, C. Veit, Z. Ma, U. Wuerfel, H. Zhu, W. Hu, F. Zhang, *Macromolecules* **2011**, *44*, 7617–7624.
[21] A. Baheti, K. R. J. Thomas, C.-P. Lee, C.-T. Li, K.-C. Ho, *J. Mater. Chem.* **2014**, *2*, 5766.
[22] Y.-D. Lin, T. J. Chow, *J. Mater. Chem.* **2011**, *21*, 14907–14916.
[23] X. Cheng, S. Sun, M. Liang, Y. Shi, Z. Sun, S. Xue, *Dyes Pigm.* **2012**, *92*, 1292–1299.
[24] S. Paek, H. Choi, H. Choi, C.-W. Lee, M.-s. Kang, K. Song, M. K. Nazeeruddin, J. Ko, *J. Phys. Chem. C* **2010**, *114*, 14646–14653.
[25] J.-B. Jorcin, M. E. Orazem, N. Pébère, B. Tribollet, *Electrochim. Acta* **2006**, *51*, 1473–1479.
[26] R. Kern, R. Sastrawan, J. Ferber, R. Stangl, J. Luther, *Electrochim. Acta* **2002**, *47*, 4213–4225.
[27] A. S. Bondarenko, G. A. Ragoisha, *Progress in Chemometrics Research*, Nova Science Publishers, New York, **2005**.
[28] S. Ito, P. Chen, P. Comte, M. K. Nazeeruddin, P. Liska, P. Péchy, M. Grätzel, *Prog. Photovoltaics* **2007**, *15*, 603–612.

Received: May 11, 2015
Published Online: July 24, 2015

